Magnetization net moment recovery with help of Fourier and Kelvin transforms

Laurent Baratchart, Juliette Leblond, Dmitry Ponomarev

August 12, 2015

1 Fourier method to recover tangential components of the net moment

We assume that the magnetization $\mathbf{M}(\mathbf{x}) = (M_1(\mathbf{x}), M_2(\mathbf{x}), M_3(\mathbf{x}))^T$, $\mathbf{x} := (x_1, x_2)^T$ is supported on a rectangular set Q with diagonal[1] q of the horizontal plane at $x_3 = 0$ with its center at the origin. Denote the net moment that we wish to recover as $\mathbf{m} := (m_1, m_2, m_3)^T = \iint_Q \mathbf{M}(\mathbf{x})\, dx_1 dx_2$.

The vertical component[2] of the magnetic field produced by the magnetization is [3, 4]

$$B_z(\mathbf{x}, x_3) = -\frac{1}{4\pi} \iint_Q \left[x_3 \left(M_1(\mathbf{t}) \frac{\partial}{\partial x_1} + M_2(\mathbf{t}) \frac{\partial}{\partial x_2} \right) + M_3(\mathbf{t}) \frac{\partial}{\partial x_3} x_3 \right] \left(|\mathbf{x} - \mathbf{t}|^2 + x_3^2 \right)^{-3/2} dt_1 dt_2. \tag{1}$$

In particular, the field is measured on the horizontal plane above the magnetic sample at height $x_3 = h$ where it equals

$$B_z(\mathbf{x}, h) = \frac{1}{4\pi} \iint_Q \frac{3h\left[M_1(\mathbf{t})(x_1 - t_1) + M_2(\mathbf{t})(x_2 - t_2)\right] + M_3(\mathbf{t}) \left[2h^2 - (x_1 - t_1)^2 - (x_2 - t_2)^2 \right]}{\left[(x_1 - t_1)^2 + (x_2 - t_2)^2 + h^2 \right]^{5/2}} dt_1 dt_2. \tag{2}$$

Taking its Fourier transform[3] and recalling that

$$\mathcal{F}\left[\frac{h}{2\pi \left(x_1^2 + x_2^2 + h^2 \right)^{3/2}} \right](\mathbf{k}) = e^{-2\pi h |\mathbf{k}|}, \quad \mathbf{k} = (k_1, k_2)^T \in \mathbb{R}^2,$$

we obtain

$$\hat{B}_z(\mathbf{k}, h) = \pi e^{-2\pi h |\mathbf{k}|} \left[i k_1 \hat{M}_1(\mathbf{k}) + i k_2 \hat{M}_2(\mathbf{k}) + |\mathbf{k}| \hat{M}_3(\mathbf{k}) \right]. \tag{3}$$

The observation $\hat{\mathbf{M}}(0) = \mathbf{m}$ suggests that the moments can be recovered from a fit of the Fourier transform of

[1] Such a weird characterization of the rectangle is only for the sake of introducing a parameter measuring its linear size. In fact, the presented results will remain true for any bounded set localized near the origin.

[2] To be consistent with other notation, we would need to denote it as $B_3(\mathbf{x}, x_3)$, however, we will still go with more physical $B_z(\mathbf{x}, x_3)$.

[3] We use the following convention for the Fourier transform: $\hat{f}(\mathbf{k}) = \mathcal{F}[f](\mathbf{k}) = \iint_{\mathbb{R}^2} e^{2\pi i (k_1 x_1 + k_2 x_2)} f(\mathbf{x})\, dx_1 dx_2$.

the measured data near the origin $\mathbf{k} = \mathbf{0}$:

$$\text{Im } \hat{B}_z(\mathbf{k}, h) \simeq \pi e^{-2\pi h|\mathbf{k}|} [k_1 m_1 + k_2 m_2], \tag{4}$$

$$\text{Re } \hat{B}_z(\mathbf{k}, h) \simeq \pi e^{-2\pi h|\mathbf{k}|} |\mathbf{k}| m_3. \tag{5}$$

However, such possibility is not realistic since the left-hand sides here cannot be explicitly computed due to the fact that the measured field $B_z(\mathbf{x}, h)$ is only partially available: we assume these measurements to be given on the square $T = [-A, A] \times [-A, A]$ centered above the origin $\mathbf{x} = \mathbf{0}$.

Even though the field decays with the distance from the magnetization support, extending the measurements with zero is natural but not necessarily the best idea when it comes to fitting near $\mathbf{k} = \mathbf{0}$. Indeed, extension of the field $B_z(\mathbf{x}, h)$ by zero outside of T results in $\hat{B}_z(\mathbf{k}, h)$ being a smooth function[4] whereas the right-hand side of (3) is, clearly, not a C^1 function at the origin, exactly where the fitting has to be done. Of course, when the measurement area T is large, the fit is expected to be better, though it will never be perfect in the closest vicinity of $\mathbf{k} = \mathbf{0}$ due to the described above fundamental discrepancy.

We illustrate this on the synthethic example with 3 dipoles with the moments $\mathbf{m}^{(1)} = (-1.0, -0.7, 1.0)^T$, $\mathbf{m}^{(2)} = (-0.6, 0.2, 0.8)^T$, $\mathbf{m}^{(3)} = (0.3, -0.9, -0.4)^T$ placed at the locations $\mathbf{x}^{(1)} = (0, 0)^T$, $\mathbf{x}^{(2)} = (0.8, -1.0)^T$, $\mathbf{x}^{(3)} = (-4.0, 3.5)^T$ in the plane $x_3 = 0$. By superposition of dipolar fields, this produces the following field at height $x_3 = h$

$$B_z(\mathbf{x}, h) = \frac{1}{4\pi} \sum_{l=1}^{3} \frac{3h\left(m_1^{(l)} x_1^{(l)} + m_2^{(l)} x_2^{(l)}\right) + m_3^{(l)} \left(2h^2 - \left(x_1^{(l)}\right)^2 - \left(x_2^{(l)}\right)^2\right)}{\left(\left(x_1^{(l)}\right)^2 + \left(x_2^{(l)}\right)^2 + h^2\right)^{5/2}},$$

which we artificially chop by setting it to zero outside of T. With this, we compute the left-hand sides of (4)-(5) on the k_1 and k_2 axes whereas in the right-hand sides we take $m_n = \sum_{l=1}^{3} m_n^{(l)}$, $n = 1, 2, 3$. On Figures 1-4, we compare matching of both sides of the equations for relatively small and large values of the measurement area dimension A while keeping the measurement plane height $h = 5$ fixed.

As it is anticipated, we observe that we would potentially be able to retrieve moments if we do the fitting in an appropriate neighborhood: sufficiently close yet not at the immediate proximity to the origin $\mathbf{k} = \mathbf{0}$ where, by cutting the original field to zero, no matter how far, we are never able to resolve a finer behavior in Fourier domain already at the level of matching smoothness properties at the point of interest. Fitting of the imaginary parts (left- and right-hand sides of (4)) is satisfactory while the discrepancy in the real parts (left- and right-hand sides of (5)) is rather dramatic especially when the measurement area is more restricted. Therefore, in the real-world setting, with this approach we expect to be able to recover only tangential components of the net moment. The failure to efficiently match the real parts and recover the normal component of the net moment m_3 is due to the presence of

[4] Recall the Paley-Wiener theorem [6], or simply perform direct computation of the Fourier transform yielding convolution with sinc functions which are analytic.

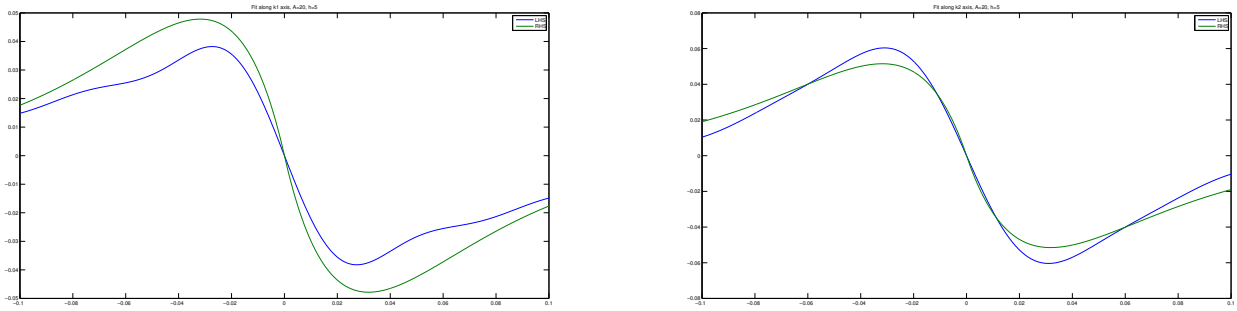

Figure 1: Matching of LHS & RHS along k_1 (left) and k_2 (right) axes for equation (4), $A = 20$

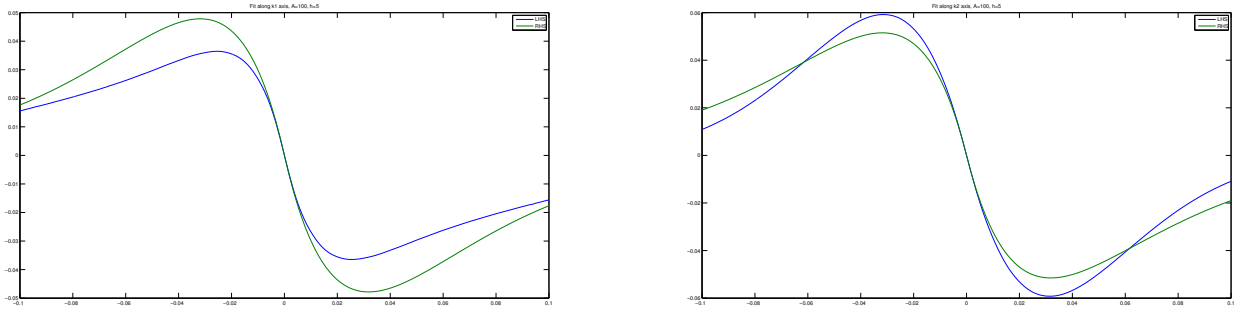

Figure 2: Matching of LHS & RHS along k_1 (left) and k_2 (right) axes for equation (4), $A = 100$

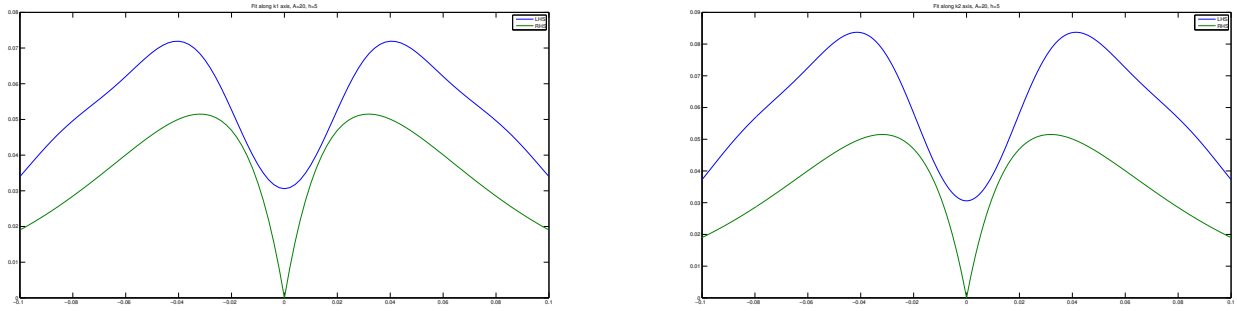

Figure 3: Matching of LHS & RHS along k_1 (left) and k_2 (right) axes for equation (5), $A = 20$

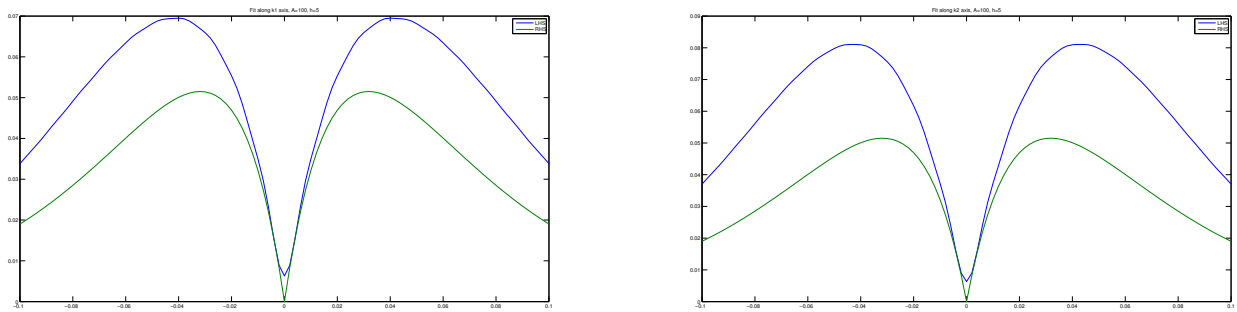

Figure 4: Matching of LHS & RHS along k_1 (left) and k_2 (right) axes for equation (5), $A = 100$

non-smooth factor $|\mathbf{k}|$ while for the imaginary parts non-smoothness manifests itself weaker since it enters only the factor $e^{-2\pi h|\mathbf{k}|}$ which is close to 1 in vicinity of the origin.

We will return to the non-smoothness issue and succeed in overcoming it in Section 3. Meanwhile, in the next section, we attempt to improve recovery of the normal component of the net moment by other means.

2 Towards recovering of the normal component, Kelvin transform

We are going to design an alternative method to recover the normal component of the moment in a more robust (meaning less measurements demanding) way. The idea is based on the Poisson representation formula for harmonic functions on the ball and dipolar approximation of the magnetic field at infinity.

Recall that in the complex plane, the Moebius transform $\dfrac{z-i}{z+i}$ sending the upper half-plane $\operatorname{Im} z > 0$ onto the unit disk $|z| < 1$ preserves harmonicity. Kelvin transforms generalize this to higher dimensions. In particular, we consider a transformation that maps the horizontal plane $x_3 = h$ with available measurements onto the unit sphere $\mathbb{S}$ while the infinitely far away point is mapped to its south pole $\boldsymbol{s} = (0,0,-1)^T$. That is, if $f(\mathbf{x}, x_3)$ is harmonic in the half-space $x_3 > h$, then $\mathcal{K}[f](\boldsymbol{\xi}) = \dfrac{1}{|\boldsymbol{\xi} - \boldsymbol{s}|} f(\mathcal{R}\boldsymbol{\xi})$, $\boldsymbol{\xi} = (\xi_1, \xi_2, \xi_3)^T$ is harmonic inside the unit ball $|\boldsymbol{\xi}| < 1$, where

$$\mathcal{R}\boldsymbol{\xi} = \left(\frac{c_0^2 \xi_1}{\xi_1^2 + \xi_2^2 + (\xi_3+1)^2}, \frac{c_0^2 \xi_2}{\xi_1^2 + \xi_2^2 + (\xi_3+1)^2}, -1 + \frac{c_0^2 (\xi_3+1)}{\xi_1^2 + \xi_2^2 + (\xi_3+1)^2} \right)^T$$

is the reflection with respect to the sphere of radius $c_0 = \sqrt{2(1+h)}$ centered at $(0,0,-1)$.

A bit of fiddling around with tedious but straightforward computations allows us to establish the following identities for the normal and tangential derivatives, valid for $\boldsymbol{\xi} \in \mathbb{S}$:

$$\mathcal{K}[\partial_{x_3} f](\boldsymbol{\xi}) = -\frac{1}{c_0^2}(\xi_3+1)\left(\mathcal{K}[f](\boldsymbol{\xi}) + 2\partial_n \mathcal{K}[f](\boldsymbol{\xi})\right), \tag{6}$$

$$\mathcal{K}[x_2 \partial_{x_1} f - x_1 \partial_{x_2} f](\boldsymbol{\xi}) = \xi_2 \partial_{\xi_1} \mathcal{K}[f](\boldsymbol{\xi}) - \xi_1 \partial_{\xi_2} \mathcal{K}[f](\boldsymbol{\xi}). \tag{7}$$

Equation (6) is analogous to the one formulated for another Kelvin transform sending interior of the sphere to its exterior and which can be found in [1, 2]. The second equation (7), in fact, shows commutation of Kelvin transform with the azimuthal angle derivative and consequently suggests the validity of the useful relation

$$\mathcal{K}\left[\int_0^{2\pi} f(\rho\cos\varphi, \rho\sin\varphi, h)\, d\varphi\right](\boldsymbol{\xi}) = \int_0^{2\pi} \mathcal{K}[f](\boldsymbol{\xi})\, d\phi, \quad \xi \in \mathbb{S}, \tag{8}$$

where $\rho = \sqrt{x_1^2 + x_2^2}$, $\varphi = \arctan\dfrac{x_2}{x_1}$, $\phi = \arctan\dfrac{\xi_2}{\xi_1}$, which indeed holds true, as can be easily checked.

Assuming, at first, that we have the data available in the whole measurement plane, we apply the described Kelvin transform to the field $B_z(\boldsymbol{x}, h)$ and, in what follows, agree to denote the resulting function as $\mathcal{K}[B_z](\boldsymbol{\xi})$, in other cases the argument of B_z will be precisely specified.

Then, the Poisson representation formula provides the unique harmonic extension into the interior of the unit ball $\mathbb{B}$:

$$F(\boldsymbol{\eta}) = \frac{1-|\boldsymbol{\eta}|^2}{4\pi} \iint_{\mathbb{S}} \frac{\mathcal{K}[B_z](\boldsymbol{\xi})}{|\boldsymbol{\xi}-\boldsymbol{\eta}|^{3/2}} d\sigma_\xi, \quad \boldsymbol{\eta} \in \mathbb{B},$$

where $d\sigma_\xi = \sin\theta d\theta d\phi$, $\theta = \arctan \dfrac{\sqrt{\xi_1^2+\xi_2^2}}{\xi_3}$ is a non-normalized Lebesgue measure on the unit sphere.

This representation significantly simplifies on the vertical axis $\eta_1 = \eta_2 = 0$, $-1 < \eta_3 < 1$

$$F(0,0,\eta_3) = \frac{1-\eta_3^2}{4\pi} \int_{-1}^{1} \frac{\Lambda^\star(\xi_3)}{(1-2\xi_3\eta_3+\eta_3^2)^{3/2}} d\xi_3, \tag{9}$$

where $\Lambda^\star(\xi_3) := \int_0^{2\pi} \mathcal{K}[B_z](\boldsymbol{\xi})\, d\phi$. Moreover, employing (8), we can express

$$\Lambda^\star(\xi_3) = \mathcal{K}\left[\int_0^{2\pi} B_z(\rho\cos\varphi, \rho\sin\varphi, h)\, d\varphi\right](\xi_3) = \mathcal{K}[\Lambda](\boldsymbol{\xi}),$$

where $\Lambda(\rho) := \int_0^{2\pi} B_z(\rho\cos\varphi, \rho\sin\varphi, h)\, d\varphi$ is essentially the angular average of the measured field.

We can notice now that in the sufficiently small positive neighborhood of $(\eta_3+1)=0$, that is when $\eta_3 \simeq -1^+$, the left-hand side of (9), being the Kelvin transform of magnetic field above height h, contains information exclusively on the net moment m_3. This can be seen as follows. From a distant point, the magnetic field of a compactly supported sample must be identical to the dipolar one with the moment equal to the net moment of the sample. In particular, on the vertical axis it depends only on the normal component of the net moment. We can also get this asymptotical result directly from (1):

$$B_z(\mathbf{0}, x_3) = -\frac{1}{4\pi x_3^3} \iint_Q \frac{3(M_1(\mathbf{t})\, t_1/x_3 + M_2(\mathbf{t})\, t_2/x_3) - 2M_3(\mathbf{t}) \left(1 - \dfrac{t_1^2+t_2^2}{2x_3^2}\right)}{\left(1+\dfrac{t_1^2+t_2^2}{2x_3^2}\right)^{5/2}} dt_1 dt_2 \simeq \frac{m_3}{2\pi x_3^3} \tag{10}$$

for $x_3 \gg q$ (and hence $\dfrac{|t_1|}{x_3}, \dfrac{|t_2|}{x_3} \ll 1$ in the integral; recall that q measures the size of the magnetization support of the sample).

Computing Kelvin transform of this, equation (9), in vicinity of $\eta_3 = -1$, becomes

$$\frac{m_3}{2\pi} \frac{(1+\eta_3)^2}{(c_0^2-\eta_3-1)^3} \simeq \frac{1-\eta_3^2}{4\pi} \int_{-1}^{1} \frac{\Lambda^\star(\xi_3)}{(1-2\xi_3\eta_3+\eta_3^2)^{3/2}} d\xi_3$$

$$\Rightarrow \quad \frac{m_3}{2\pi} \frac{(1+\eta_3)}{(c_0^2-\eta_3-1)^3} \simeq \frac{1-\eta_3}{4\pi} \int_{-1}^{1} \frac{\Lambda^\star(\xi_3)}{(1-2\xi_3\eta_3+\eta_3^2)^{3/2}} d\xi_3. \tag{11}$$

Let us pause for a minute and analyze the equation (11). We notice that while vanishing of its left-hand side at

$\eta_3 = -1$ is immediate, it is not obvious at all that

$$\lim_{\eta_3 \to -1^+} \int_{-1}^{1} \frac{\Lambda^\star(\xi_3)}{\left(1 - 2\xi_3\eta_3 + \eta_3^2\right)^{3/2}} d\xi_3 = 0, \tag{12}$$

and generally it is false. The natural question is then: under which assumptions on $B_z(\mathbf{x}, h)$ does this hold? Interestingly enough, the answer encodes the fact that the measured magnetic field should be the restriction of the gradient of a harmonic function! In fact, it hinges on the equivalence

$$\iint_{\mathbb{R}^2} B_z(\mathbf{x}, h)\, dx_1 dx_2 = 0 \quad \Longleftrightarrow \quad \iint_{\mathbb{S}} \frac{\mathcal{K}[B_z](\boldsymbol{\xi})}{\left(1 + \xi_3\right)^{3/2}} d\sigma_\xi = 0, \tag{13}$$

which is due to the Jacobian in the change of variable $dx_1 dx_2 = \dfrac{1}{\left(1 + \xi_3\right)^2} d\sigma_\xi$. Therefore, (12) would be established if we could pass to the limit inside the integral sign. This can be done under assumption that $\Lambda^\star(\xi_3) = \mathcal{O}\left(\left(1 + \xi_3\right)^\alpha\right)$ near $\xi_3 = -1$ for some $\alpha > \dfrac{1}{2}$. Indeed, we can justify the limit passing by applying the dominated convergence theorem [6] once we can bound the integrand by a L^1_{loc} function at $\eta_3 = -1$. But this is feasible since, for $-1 < \xi_3 < 0$,

$$1 - 2\xi_3\eta_3 + \eta_3^2 = \left(\eta_3 - \xi_3\right)^2 + 1 - \xi_3^2 \geq \left(1 + \xi_3\right)\left(1 - \xi_3\right),$$

and hence, for $\alpha > \dfrac{1}{2}$,

$$\int_{-1}^{0} \frac{\left|\Lambda^\star(\xi_3)\right|}{\left(1 + \xi_3\right)^{\frac{3}{2} - \alpha} \left(1 - \xi_3\right)^{\frac{3}{2}}} d\xi_3 < \infty.$$

Therefore, recalling (13), we deduce

$$\lim_{\eta_3 \to -1^+} \int_{-1}^{1} \frac{\Lambda^\star(\xi_3)}{\left(1 - 2\xi_3\eta_3 + \eta_3^2\right)^{3/2}} d\xi_3 = \frac{1}{2^{3/2}} \int_{-1}^{1} \frac{\Lambda_0^\star(\xi_3)\left(1 + \xi_3\right)^\alpha}{\left(1 + \xi_3\right)^{3/2}} d\xi_3 = 0.$$

Note that the assumed vanishing behavior of $\Lambda^\star(\xi_3)$ near $\xi_3 = -1$ is equivalent to certain rapidness of the radial decay at infinity of $B_z(\mathbf{x}, h)$. In case of clean measurements, i.e. when the measured field is noise-free so that is is consistent with (2) for some magnetization distribution $\mathbf{M}(\mathbf{x})$, we have $B_z(\mathbf{x}, h) = \mathcal{O}\left(1/\left|\mathbf{x}\right|^3\right)$ as $|\mathbf{x}| \to \infty$ and since $\mathcal{R}\left[\sqrt{x_1^2 + x_2^2}\right](\boldsymbol{\xi}) = \dfrac{c_0^2}{2}\sqrt{\dfrac{1 - \xi_3}{1 + \xi_3}}$, the assumption on $\Lambda^\star(\xi_3)$ is valid with $\alpha = 1$. It is needless to say that the form of the field (2) also certainly implies validity of the assumption on the left of (13). We conclude this small piece of analysis with the remark that the made observations may give us a hint on how to denoise the measurements in a physically meaningful way consistent with our model.

Now, assuming ideal measurements, we write

$$\Lambda^\star(\xi_3) = \left(1 + \xi_3\right)\Lambda_0^\star(\xi_3) \tag{14}$$

for some $\Lambda_0^\star \in C([-1, 1])$ in order to incorporate the decay property (as discussed, $\alpha = 1$). We go back to the

computational strategy and notice that, from (11), it is tempting to get an explicit expression for the net moment component m_3 by differentiating both sides at $\eta_3 = -1$. We embark on exploring this possibility.

Taking into account (14), we apply $\left.\dfrac{d}{d\eta_3}\right|_{\eta_3=-1}$ operator to both sides of (11)

$$\frac{m_3}{2\pi c_0^6} = \frac{1}{4\pi}\lim_{\eta_3\to -1^+}\int_{-1}^{1}\frac{(1+\xi_3)\,\Lambda_0^\star(\xi_3)}{(1-2\xi_3\eta_3+\eta_3^2)^{3/2}}d\xi_3 + \frac{3}{2\pi}\lim_{\eta_3\to -1^+}\int_{-1}^{1}\frac{(1+\xi_3)\,(\xi_3-\eta_3)\,\Lambda_0^\star(\xi_3)}{(1-2\xi_3\eta_3+\eta_3^2)^{5/2}}d\xi_3.$$

The first term here vanishes thanks to (12) while the second one must be handled with special care since it is clear that we cannot simply pass to the limit inside the integral, it would otherwise imply that it is also zero by the same argument based on (13) yielding in total the overall absurd result $m_3 = 0$. The remedy to the situation is integration by parts

$$\begin{aligned}\frac{m_3}{2\pi c_0^6} &= -\frac{1}{2\pi}\lim_{\eta_3\to -1^+}\int_{-1}^{1}(1+\xi_3)\,(\xi_3-\eta_3)\,\Lambda_0^\star(\xi_3)\,\partial_{\xi_3}\frac{1}{(1-2\xi_3\eta_3+\eta_3^2)^{3/2}}d\xi_3\\ &= \frac{1}{4\pi}\left[-\Lambda_0^\star(1)+\frac{1}{\sqrt{2}}\int_{-1}^{1}\frac{\Lambda_0^\star(\xi_3)}{(1+\xi_3)^{1/2}}d\xi_3+\frac{1}{\sqrt{2}}\int_{-1}^{1}(1+\xi_3)^{1/2}\,\partial_{\xi_3}\Lambda_0^\star(\xi_3)\,d\xi_3\right.\\ &+ \left. 2\lim_{\eta_3\to -1^+}\int_{-1}^{1}\frac{(\xi_3-\eta_3)\,\Lambda_0^\star(\xi_3)}{(1-2\xi_3\eta_3+\eta_3^2)^{3/2}}d\xi_3\right].\end{aligned}$$

The second term in the square braces is zero for the same reason as before and so is the main part of the third one - its integration by parts produces only a boundary value which exactly cancels out the very first term $-\Lambda_0^\star(1)$. The last term looks similar to the vanishing one, however, we cannot justify passing to the limit and, in fact, the result of such a naive limit passage will be false (unless, of course, $\Lambda_0^\star(-1) = 0$). We treat this problematic term with integration by parts again that yields

$$\frac{m_3}{2\pi c_0^6} = \frac{1}{2\pi}\left[-\Lambda_0^\star(1)-\Lambda_0^\star(-1)+\lim_{\eta_3\to -1^+}\int_{-1}^{1}\frac{(\xi_3-\eta_3)\,\partial_{\xi_3}\Lambda_0^\star(\xi_3)+\Lambda_0^\star(\xi_3)}{(1-2\xi_3\eta_3+\eta_3^2)^{1/2}}d\xi_3\right] = -\frac{1}{2\pi}\Lambda_0^\star(-1),$$

since the dominated convergence theorem can already be applied to allow passing to the limit in the last term in the braces. The obtained result means that the information on the normal component of net moment is entirely contained in the radial asymptotics of the measured field

$$m_3 = -\frac{c_0^6}{\sqrt{2}}\lim_{\xi_3\to -1^+}\frac{1}{(1+\xi_3)^{3/2}}\Lambda\left(\frac{c_0^2}{2}\sqrt{\frac{1-\xi_3}{1+\xi_3}}\right). \tag{15}$$

This expression may at first glance look striking because it does not incorporate data on the whole measurement plane, instead it involves only the integrals of $B_z(\mathbf{x}, h)$ over circles of infinitely large radii. Even though this solves the problem in the ideal case of complete data, in practice those distant circles are exactly where we necessarilly lack measurements. Therefore, with this approach, we are facing the same features of the problem as with the Fourier method, nevertheless, matching of the left- and right-hand sides of (11) illustrated on Figure 5 looks doubtfully

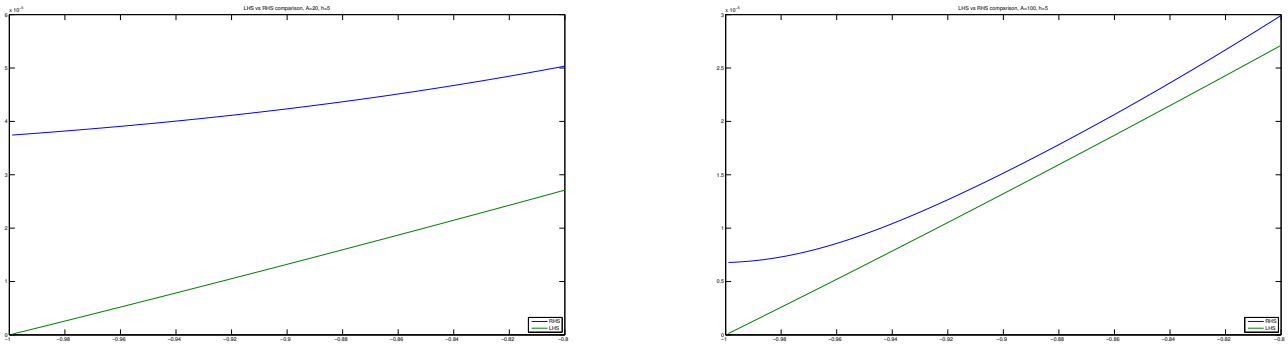

Figure 5: Matching of LHS & RHS for (11), $A = 20$ (left) and $A = 100$ (right)

better as compared to proximity of curves in Figures 3-4. For this computations, performed for the same synthetic example as before, to mimic the realistic situation of restricted measurements, the lower limit of integration -1 in the right-hand side of (11) was replaced with $\xi_0 := \dfrac{c_0^4 - 4A^2}{c_0^4 + 4A^2}$ which corresponds to cutting the original field to zero outside of the disk of radius A in the measurement plane. Then we observe, as expected, divergence of the curves: near the origin due to the cut of the measured data whereas for larger values of η_3 due to the breakdown of the single dipolar approximation.

Despite the seemingly sad end of the journey for finding an explicit form of m_3, this tells us more than that we should only be content with matching of the left- and right-hand sides of (11) in some wisely chosen neighborhood of $\eta_3 = -1$, it gives us a clue on how to extend the measured field. Indeed, the result (15) is not surprising, it just reveals the fact that at distant points on the measurement plane the field should look dipolar with the moment equal to the net moment of a compactly supported sample - similarly to the vertical asymptotics (10), we can obtain the horizontal ones from (2), for $|\mathbf{x}| \gg q$,

$$B_z(\mathbf{x}, h) \simeq \frac{1}{4\pi\left(x_1^2 + x_2^2 + h^2\right)^{5/2}} \iint_Q \left[3h\left(x_1 M_1(\mathbf{t}) + x_2 M_2(\mathbf{t})\right) - \left(x_1^2 + x_2^2 - 2h^2\right) M_3(\mathbf{t})\right] dt_1 dt_2 \tag{16}$$

$$\simeq \frac{m_3\left(2h^2 - x_1^2 - x_2^2\right)}{4\pi\left(x_1^2 + x_2^2 + h^2\right)^{5/2}}, \tag{17}$$

or, in a more crude manner,

$$B_z(\mathbf{x}, h) \simeq -\frac{m_3}{4\pi\left(x_1^2 + x_2^2\right)^{3/2}}. \tag{18}$$

This suggests that we could complete the measured field if we knew the net moment component m_3. Assuming the measurement area T to be large enough such that outside of it the field will look dipolar, and thus be well-

represented by the expression (17), we rewrite the integral on the right of (11) by splitting it into two parts

$$\begin{aligned}\frac{m_3}{2\pi}\frac{(1+\eta_3)}{\left(c_0^2-\eta_3-1\right)^3} &\simeq -\frac{m_3\,(1-\eta_3)}{8\sqrt{2}\pi}\int_{-1}^{\xi_0}\frac{(\xi_3+1)\left(c_0^4-2\left(c_0^2-2\right)^2-\left(c_0^4+2\left(c_0^2-2\right)^2\right)\xi_3\right)}{\left[c_0^4+\left(c_0^2-2\right)^2-4\left(c_0^2-1\right)\xi_3\right]^{5/2}\left(1-2\xi_3\eta_3+\eta_3^2\right)^{3/2}}d\xi_3\\ &+\frac{1-\eta_3}{4\pi}\int_{\xi_0}^{1}\frac{\Lambda^\star\left(\xi_3\right)}{\left(1-2\xi_3\eta_3+\eta_3^2\right)^{3/2}}d\xi_3\end{aligned}$$

(recall the definition $\xi_0=\dfrac{c_0^4-4A^2}{c_0^4+4A^2}$). But now if we simply rearrange the terms, we can view the resulting equation as an improved version of (11) to perform fitting

$$\frac{m_3}{2\pi}\left(\frac{(1+\eta_3)}{\left(c_0^2-\eta_3-1\right)^3}+\frac{\left[c_0^4+2\left(c_0^2-2\right)^2\right](1-\eta_3)}{64\left(c_0^2-1\right)^{5/2}\left(-\eta_3\right)^{3/2}}G_0\left(\eta_3\right)\right)\simeq\frac{1-\eta_3}{4\pi}\int_{\xi_0}^{1}\frac{\Lambda^\star\left(\xi_3\right)}{\left(1-2\xi_3\eta_3+\eta_3^2\right)^{3/2}}d\xi_3, \tag{19}$$

where

$$\begin{aligned}G_0 &:= \int_{-1}^{\xi_0}\frac{(1+x)\,(\alpha-x)}{(\beta-x)^{5/2}\,(x+\gamma)^{3/2}}dx\\ &= -\frac{2}{3}\left[\frac{(\beta+\gamma)\,(\gamma-x)\left[3\,(\beta+x)\,(\beta+\gamma)-2\,(1-\gamma)\,(\alpha+\gamma)\right]}{(\beta+\gamma)^3\,(\beta+x)^{3/2}\,(\gamma-x)^{1/2}}\right.\\ &+ \left.\frac{(2x+3\beta+\gamma)\left[(\gamma-x)\,(\beta+x)\,(\alpha-\beta+\gamma-1)-(1-\gamma)\,(\alpha+\gamma)\,(4x-3\gamma+\beta)\right]}{(\beta+\gamma)^3\,(\beta+x)^{3/2}\,(\gamma-x)^{1/2}}\right]\Bigg|_{x=-\xi_0}^{x=1},\end{aligned} \tag{20}$$

$$\alpha:=\frac{c_0^2-2\left(c_0^2-2\right)^2}{c_0^2+2\left(c_0^2-2\right)^2},\quad \beta:=\frac{c_0^4+\left(c_0^2-2\right)^2}{4\left(c_0^2-1\right)},\quad \gamma:=-\frac{1+\eta_3^2}{2\eta_3}, \tag{21}$$

and the integral computation is detailed in the Appendix (note that $\xi_0<1<\beta$ and $\gamma>1$ for $\eta_3<0$). We can now appreciate the effect of such extension by comparing the fits of right- and left-hand sides for the both equations (11) and (19) - see Figures 6 and 7, where we can observe that the correction term makes the relative error uniformly smaller in vicinity of the fitting point $\eta_3=-1$ while further away from it the correction terms produce less significant effects, as it was anticipated.

3 Improving net moment recovery in the Fourier method approach

Having concluded the previous section with the field completion idea, it is natural to go back and try out the same strategy for the previous computation performed in the Fourier domain. Interestingly enough, we observe that the corrections decouple in a sense that the corrected term due to the asymptotic dipolar extension involves only that component of the net moment for which the equation is being formulated. For example, we see that the Fourier integral of the extension of the field at the leading order is given in terms of m_3 by (18) and so this will produce a correction for the equation (5), however, when we are concerned with recovery of the tangential components, the

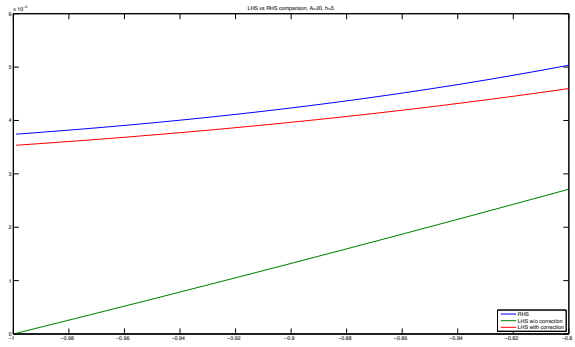

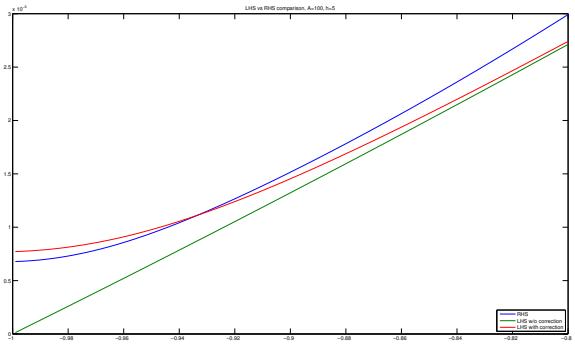

Figure 6: Matching of LHS & RHS for (19) compared to (11), $A = 20$ (left) and $A = 100$ (right)

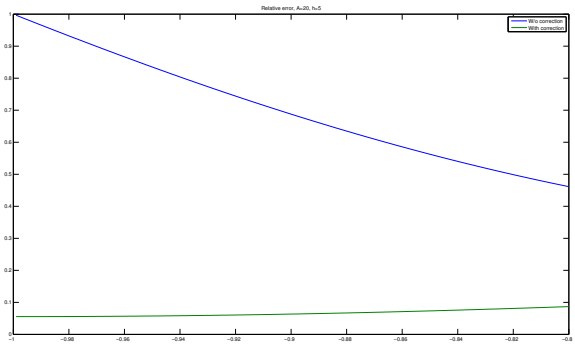

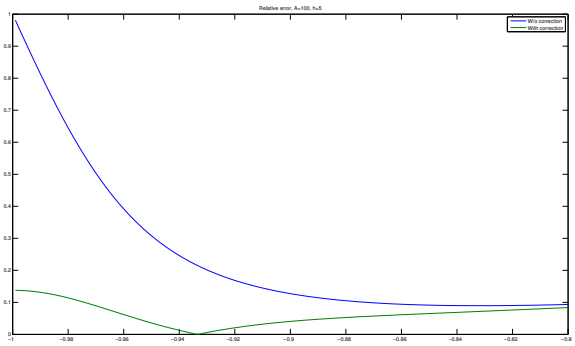

Figure 7: Relative error between matching LHS & RHS of (11) and (19), $A = 20$ (left) and $A = 100$ (right)

imaginary part of the Fourier integral vanishes

$$\mathrm{Im}\iint_{\mathbb{R}^2\backslash T}\frac{e^{2\pi i(k_1x_1+k_2x_2)}}{\left(x_1^2+x_2^2\right)^{3/2}}dx_1dx_2=\iint_{\mathbb{R}^2\backslash T}\frac{\sin\left(2\pi k_1x_1\right)\cos\left(2\pi k_2x_2\right)+\cos\left(2\pi k_1x_1\right)\sin\left(2\pi k_2x_2\right)}{\left(x_1^2+x_2^2\right)^{3/2}}dx_1dx_2=0,$$

by symmetry of the region of the integration, and we have to take the next order term in asymptotics (16) which will depend only on the tangential components of the net moment. We thus have

$$\begin{aligned}\mathrm{Im}\ \hat{B}_z\left(\mathbf{k},h\right) \ &\simeq \ \iint_T\sin\left[2\pi\left(k_1x_1+k_2x_2\right)\right]B_z\left(\mathbf{x},h\right)dx_1dx_2\\ &+\frac{3h}{4\pi}\iint_{\mathbb{R}^2\backslash T}\frac{m_1x_1\sin\left(2\pi k_1x_1\right)\cos\left(2\pi k_2x_2\right)+m_2x_2\cos\left(2\pi k_1x_1\right)\sin\left(2\pi k_2x_2\right)}{\left(x_1^2+x_2^2\right)^{5/2}}dx_1dx_2,\end{aligned}\quad(22)$$

where the second integral can be computed explicitly in terms of special functions if we crudely approximate the integration area $\mathbb{R}^2\backslash T$ by the complement of the disk of radius A and evaluate it on either k_1 or k_2 axis. We would like to stress an important fact that we can explicitly evaluate the correction integral since its numerical computation based on truncation of the infinite region or asymptotic estimation will not suffice to reproduce the desired behavior in the closest neighborhood of $\mathbf{k}=\mathbf{0}$.

Without loss of generality, let us take $k_2=0$. Then, combining (22) with (4), we obtain after rearrangement of terms and change of variable to the polar coordinates in the integral

$$\iint_T\sin\left(2\pi k_1x_1\right)B_z\left(\mathbf{x},h\right)dx_1dx_2\simeq m_1\left(\pi k_1e^{-2\pi h|k_1|}-\frac{3h}{4\pi}\int_A^\infty\int_0^{2\pi}\frac{\cos\phi\sin\left(2\pi k_1r\cos\phi\right)}{r^3}d\phi dr\right).\quad(23)$$

We now note that the integral on the right can be expressed in terms of one-dimensional integral of cylindrical functions

$$\int_0^{2\pi}\cos\phi\sin\left(2\pi k_1r\cos\phi\right)d\phi=4\int_0^{\frac{\pi}{2}}\cos\phi\sin\left(2\pi k_1r\cos\phi\right)d\phi=-\frac{1}{k_1}\partial_rJ_0\left(2\pi k_1r\right)=-2\pi J_0'\left(2\pi k_1r\right),$$

where in the second equality we used the integral representation of the Bessel function of the zeroth order

$$J_0\left(2\pi k_1r\right)=\frac{2}{\pi}\int_0^{\frac{\pi}{2}}\cos\left(2\pi k_1r\cos\phi\right)d\phi.\quad(24)$$

Employing the connection formula $J_0'\left(x\right)=-J_1\left(x\right)$ and the odd parity of this function, the integral in the left-hand side of (23) can be transformed as

$$\frac{3h}{4\pi}\int_A^\infty\int_0^{2\pi}\frac{\cos\phi\sin\left(2\pi k_1r\cos\phi\right)}{r^3}d\phi dr=\frac{3h}{2}\int_A^\infty\frac{J_1\left(2\pi k_1r\right)}{r^3}dr=\frac{3h}{2}4\pi^2k_1^2\mathrm{sgn}k_1\int_{2\pi|k_1|A}^\infty\frac{J_1\left(x\right)}{x^3}dx.$$

Finally, (23) yields a fitting equation

$$\iint_T \sin\left(2\pi k_1 x_1\right) B_z\left(\mathbf{x}, h\right) dx_1 dx_2 \simeq m_1 \pi k_1 \left(e^{-2\pi h|k_1|} + \frac{h}{2A} G_1\left(2\pi\left|k_1\right| A\right)\right), \tag{25}$$

where the correction term entering the right-hand side expresses in terms of Bessel and Struve functions [5]

$$G_1\left(x\right) := 2x - \left(3 + 2x^2\right) J_0\left(x\right) + 2x J_1\left(x\right) - J_2\left(x\right) + \pi x^2 \left(J_0\left(x\right) H_1\left(x\right) - J_1\left(x\right) H_0\left(x\right)\right), \tag{26}$$

and details of the integral computations are given in Appendix.

In a totally similar fashion, setting $k_1 = 0$ in (22), we obtain the equation involving the component m_2

$$\iint_T \sin\left(2\pi k_2 x_2\right) B_z\left(\mathbf{x}, h\right) dx_1 dx_2 \simeq m_2 \pi k_2 \left(e^{-2\pi h|k_2|} + \frac{h}{2A} G_1\left(2\pi\left|k_2\right| A\right)\right). \tag{27}$$

Now turning the focus to computations in order to recover the normal component of the net moment, we use the leading order asymptotics (18) (which is not vanishing now) and, similarly to (22), obtain

$$\begin{aligned} \text{Re } \hat{B}_z\left(\mathbf{k}, h\right) \quad \simeq \quad & \iint_T \cos\left[2\pi\left(k_1 x_1 + k_2 x_2\right)\right] B_z\left(\mathbf{x}, h\right) dx_1 dx_2 \\ & - \frac{m_3}{4\pi} \iint_{\mathbb{R}^2 \setminus T} \frac{\cos\left(2\pi k_1 x_1\right)\cos\left(2\pi k_2 x_2\right) - \sin\left(2\pi k_1 x_1\right)\sin\left(2\pi k_2 x_2\right)}{\left(x_1^2 + x_2^2\right)^{3/2}} dx_1 dx_2. \end{aligned} \tag{28}$$

As before, setting $k_2 = 0$, from (5) and (28), we get an analog of (23)

$$\iint_T \cos\left(2\pi k_1 x_1\right) B_z\left(\mathbf{x}, h\right) dx_1 dx_2 \simeq m_3 \left(\pi\left|k_1\right| e^{-2\pi h|k_1|} + \frac{1}{4\pi} \int_A^\infty \int_0^{2\pi} \frac{\cos\left(2\pi k_1 r \cos\phi\right)}{r^2} d\phi dr\right) \tag{29}$$

with the integral term on the right rewritten as

$$\frac{1}{4\pi} \int_A^\infty \int_0^{2\pi} \frac{\cos\left(2\pi k_1 r\cos\phi\right)}{r^2} d\phi dr = \frac{1}{2} \int_A^\infty \frac{J_0\left(2\pi k_1 r\right)}{r^2} dr = \pi\left|k_1\right| \int_{2\pi|k_1|A}^\infty \frac{J_0\left(x\right)}{x^2} dx,$$

where the integral representation (24) and the even parity of $J_0\left(x\right)$ were used.

We thus arrive at

$$\iint_T \cos\left(2\pi k_1 x_1\right) B_z\left(\mathbf{x}, h\right) dx_1 dx_2 \simeq m_3 \left(\pi\left|k_1\right| e^{-2\pi h|k_1|} + \frac{1}{2A} G_2\left(2\pi\left|k_1\right| A\right)\right), \tag{30}$$

where

$$G_2\left(x\right) := -x + \left(1 + x^2\right) J_0\left(x\right) - x J_1\left(x\right) - \frac{\pi x^2}{2} \left(J_0\left(x\right) H_1\left(x\right) - J_1\left(x\right) H_0\left(x\right)\right), \tag{31}$$

and all computations are again put in Appendix.

Of course, similarly, setting $k_1 = 0$ in (28), we could have as well obtained the equation on the k_2 axis:

$$\iint_T \cos(2\pi k_2 x_2)\, B_z(\mathbf{x}, h)\, dx_1 dx_2 \simeq m_3 \left(\pi |k_2| e^{-2\pi h|k_2|} + \frac{1}{2A} G_2(2\pi |k_2| A) \right). \tag{32}$$

On Figures 8-13, we observe the improved matching of the left- and right-hand sides of (25), (27), which demonstrates the quality of the upgraded recovery scheme for tangential components of the net moment, and (30), (32) - for the normal component. When the measurement area is large, the improvement is insignificant - Figures 10, 13 show no visible difference between curves representing the right-hand sides of (25) and (27) as compared to (4) evaluated on k_1 and k_2 axes, respectively, and similarly, for the equations (30), (32) compared to the evaluation from (5). The plots of relative errors computed with respect to the integrals of the field (i.e. left-hand sides) are presented on Figures 8 and show that the errors are uniformly smaller near the origin in case when the field extension is implemented. Even though the last remark may appear questionable when matching is performed for the equations involving tangential components of the net moment (25) and (27), the validity of this fact becomes evident after replotting in a smaller neighborhood of the origin - see Figures 9, 11 and 15, 17. On Figure 18, we additionally plot absolute error since Figures 11, 17 despite showing advantage of the implementation of correction terms, still contain numerical artefacts (which are, most likely, due to insufficient precision of numerical computation of the Fourier integral). In this context, we emphasize the difference in the effect of dipolar extension compared with that in case of Kelvin transform: such extension in the Fourier domain does not yield uniformly smaller error than that from simple truncation by zero as it was observed for the Kelvin transform case on Figure 7, however, the error is uniformly smaller in sufficient proximity to the origin. It is also interesting to check visually the form of correction terms, essentially, the functions (26) and (31), which, as we see on Figures 21-22, are fairly localized for larger measurements area and provide an expected remedy for the mismatch in smoothness at the origin discussed at the end of Section 3.

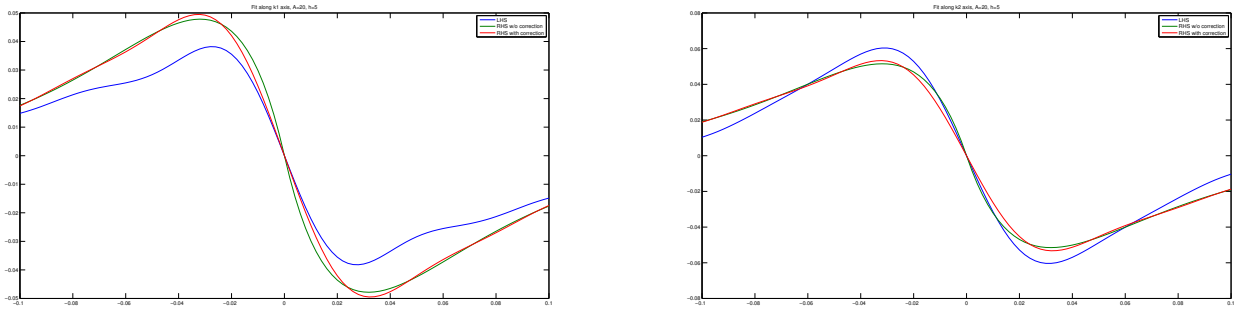

Figure 8: Matching of LHS & RHS of (25) (left) and (27) (right) compared to (4) along k_1 and k_2 axes, $A = 20$

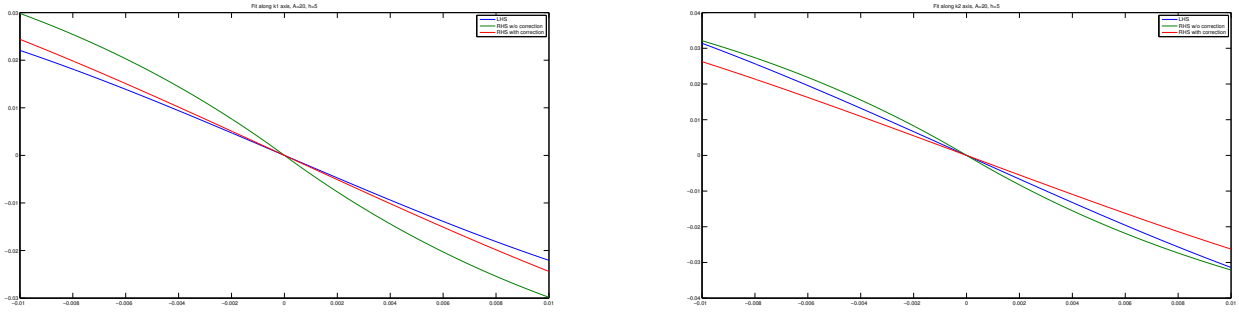

Figure 9: Matching of LHS & RHS of (25) (left) and (27) (right) compared to (4) along k_1 and k_2 axes, $A = 20$ (10 times smaller neighborhood of the origin)

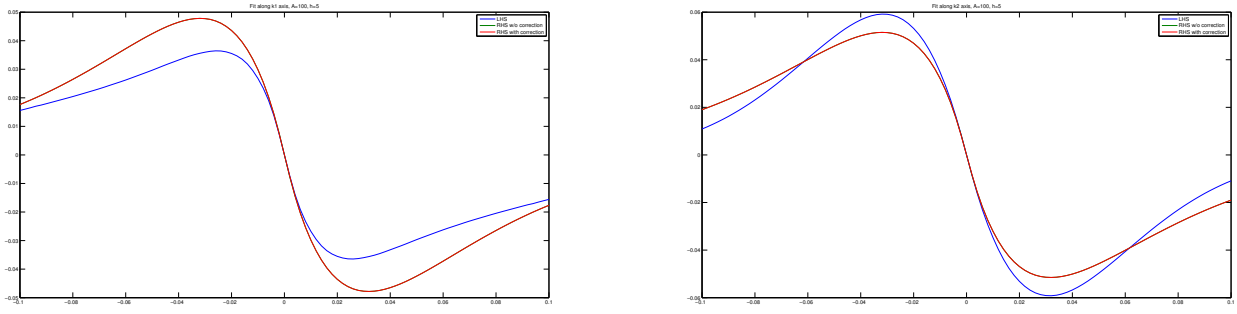

Figure 10: Matching of LHS & RHS of (25) (left) and (27) (right) compared to (4) along k_1 and k_2 axes, $A = 100$

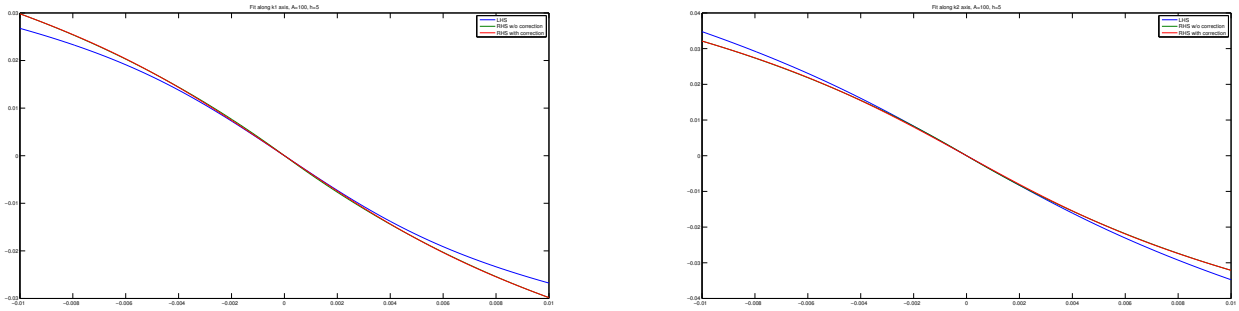

Figure 11: Matching of LHS & RHS of (25) (left) and (27) (right) compared to (4) along k_1 and k_2 axes, $A = 100$ (10 times smaller neighborhood of the origin)

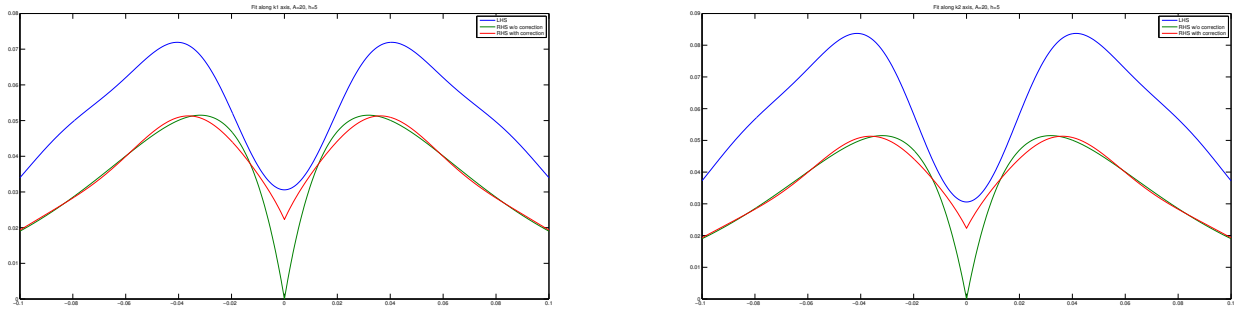

Figure 12: Matching of LHS & RHS of (30) (left) and (32) (right) compared to (5) along k_1 and k_2 axes, $A = 20$

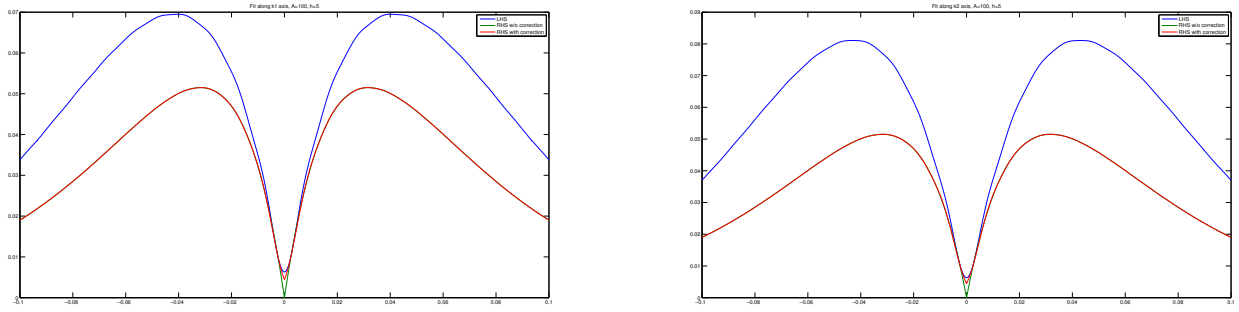

Figure 13: Matching of LHS & RHS of (30) (left) and (32) (right) compared to (5) along k_1 and k_2 axes, $A = 100$

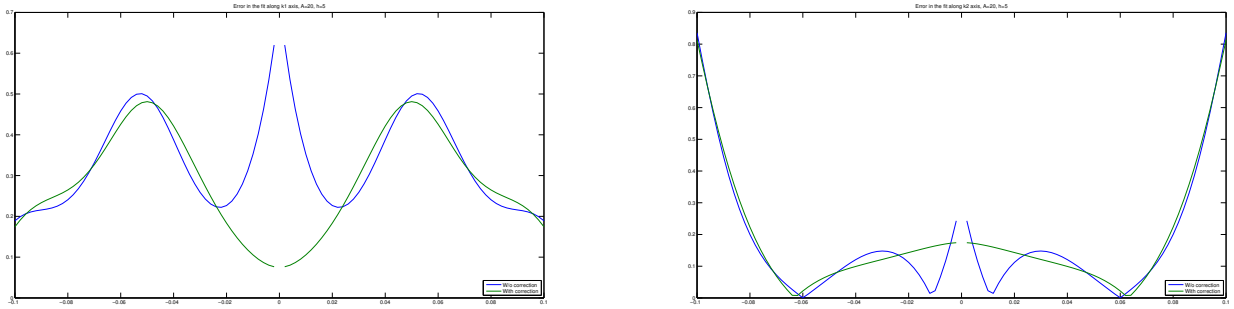

Figure 14: Relative error between matching LHS & RHS of (25) (left) and (27) (right) compared to (4) along k_1 and k_2 axes, $A = 20$

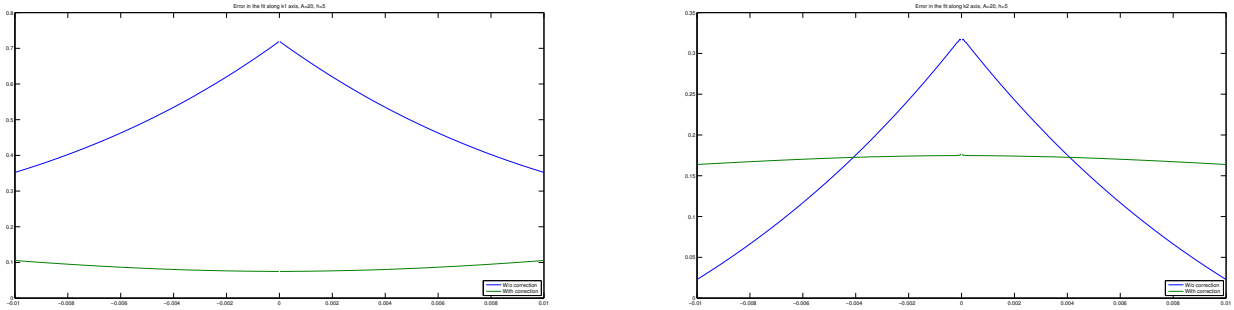

Figure 15: Relative error between matching LHS & RHS of (25) (left) and (27) (right) compared to (4) along k_1 and k_2 axes, $A = 20$ (10 times smaller neighborhood of the origin)

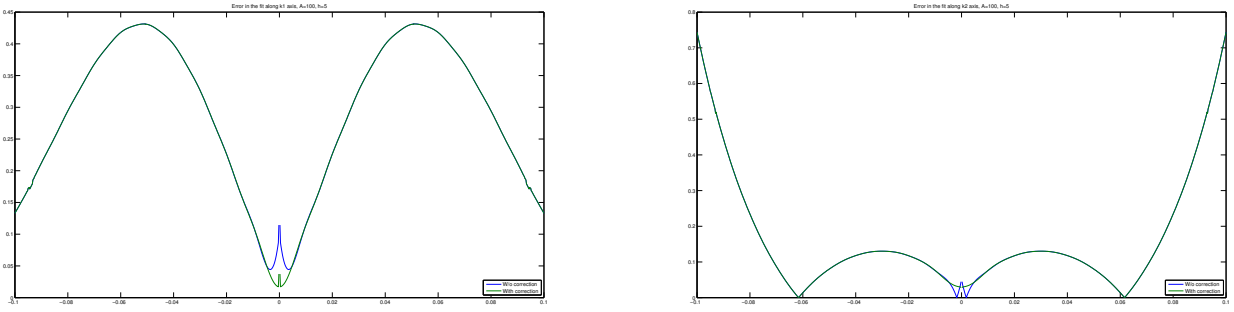

Figure 16: Relative error between matching LHS & RHS of (25) (left) and (27) (right) compared to (4) along k_1 and k_2 axes, $A = 100$

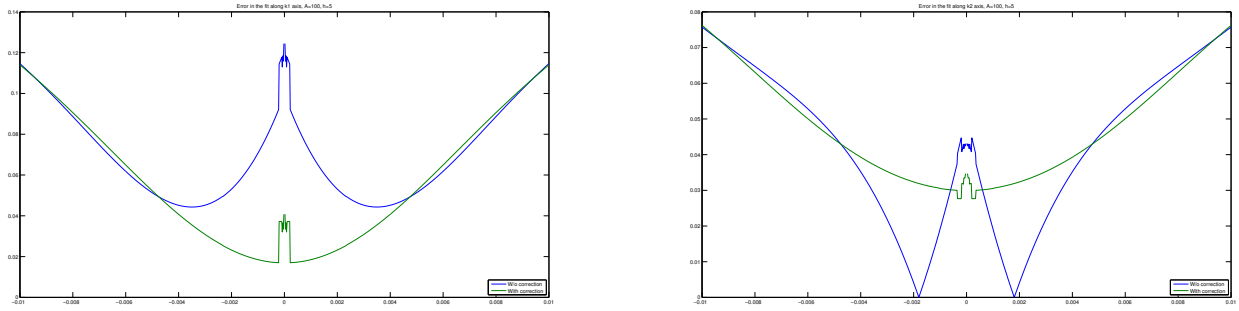

Figure 17: Relative error between matching LHS & RHS of (25) (left) and (27) (right) compared to (4) along k_1 and k_2 axes, $A = 100$ (10 times smaller neighborhood of the origin)

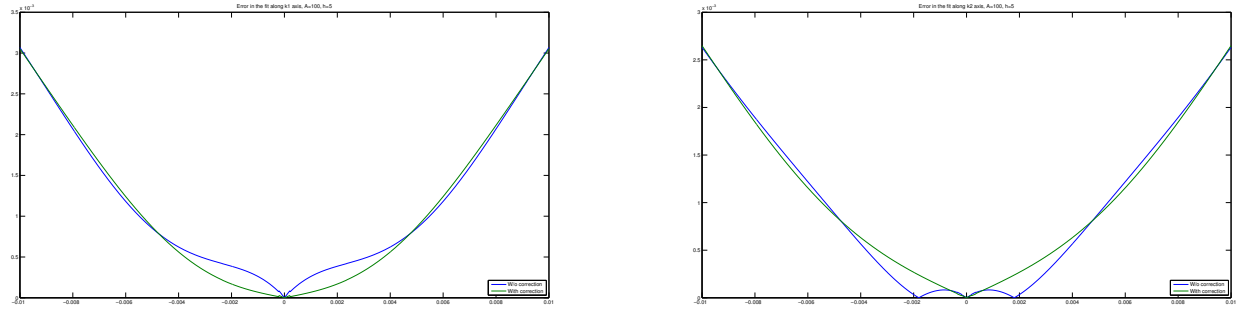

Figure 18: Absolute error between matching LHS & RHS of (25) (left) and (27) (right) compared to (4) along k_1 and k_2 axes, $A = 100$ (10 times smaller neighborhood of the origin)

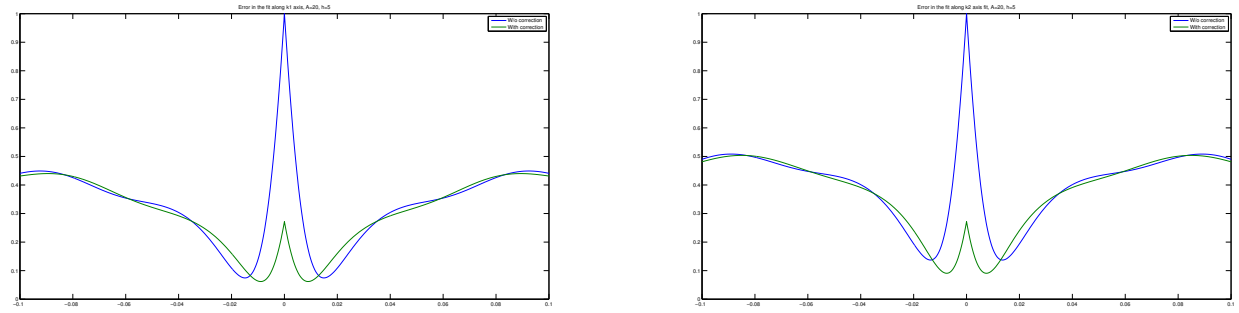

Figure 19: Relative error between matching LHS & RHS of (30) (left) and (32) (right) compared to (5) along k_1 and k_2 axes, $A = 20$

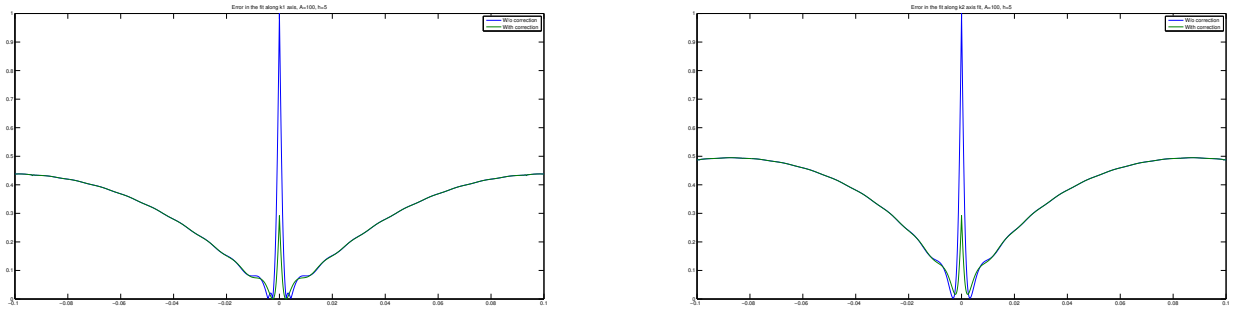

Figure 20: Relative error between matching LHS & RHS of (30) (left) and (32) (right) compared to (5) along k_1 and k_2 axes, $A = 100$

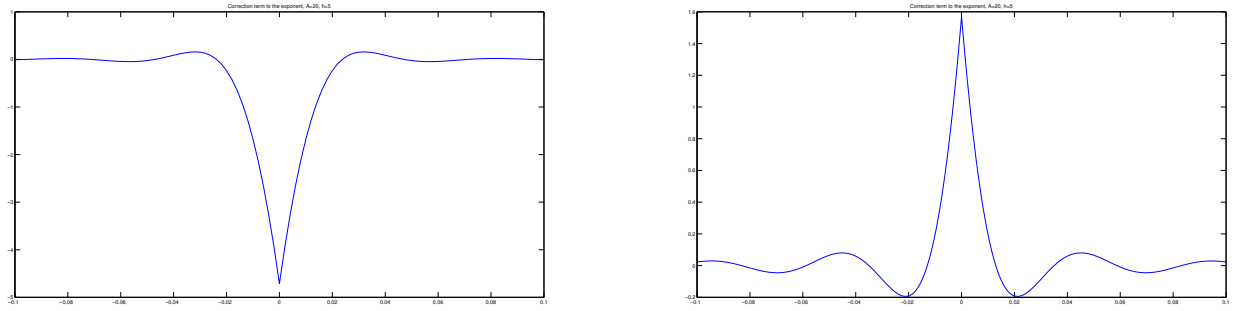

Figure 21: Correction terms in equations (25), (27) (left) and (30), (32) (right), $A = 20$

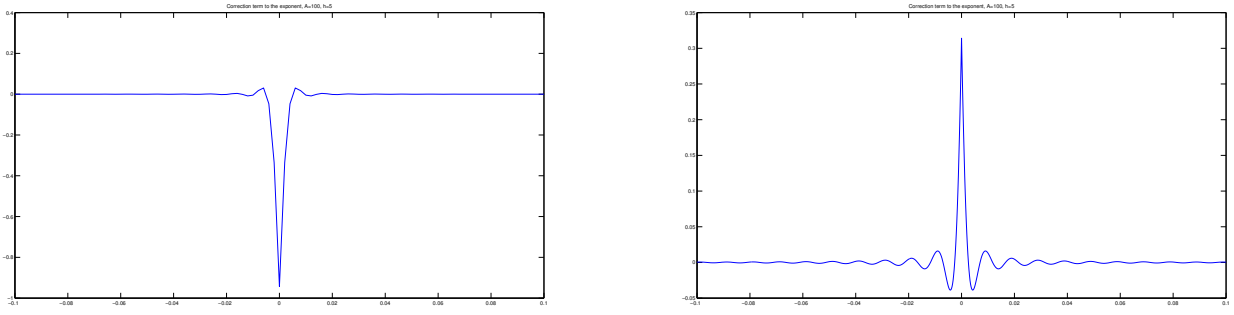

Figure 22: Correction terms in equations (25), (27) (left) and (30), (32) (right), $A = 100$

4 What is next?..

On-going work

- Checking the quality of the recovery of the net moment on synthetic examples with continuous distributions of magnetization and experimental values of parameters (measurement area and sample size, the height, magnitudes of the moments).
- Performing real numerical fitting to recover values of components of the net moment rather than observing visual matching of curves.

Further potential improvements

- Introduce an intermediate area prior to the furthest one where dipolar asymptotics is valid. We can obtain values there by a natural continuation of expansion over suitable basis (eigenfunctions of the underlying operator or simply the Poisson operator intrinsic to the problem). Perhaps suitable trade-off has to be found between number of them (governing the representation quality of the measured field) and reasonable behavior outside of the measurement area (consistent with the dipolar decay at large distances, ideally).
- In the extension, incorporate/reinforce some additionally known properties of the field such as smoothness and $\iint_{\mathbb{R}^2} B_z(\mathbf{x}, h)\, dx_1 dx_2 = 0$.
- Perform *a priori* estimation of the neighborhood size for the fitting.
- Consider improvement of the recovery of the component m_3 by performing fitting along the both k_1 and k_2 axes, i.e. employing the both (30) and (32) equations.
- In all cases, we can improve by performing fitting along surfaces rather than lines (on the axes), but the correction term integrals, most likely, will be feasible to compute only numerically.
- To incorporate all the available data, we can evaluate numerically the difference between integral of the measured field over the square T and the disk of radius A, and add this correction to the right-hand side of the fitting equations in Section 3.

Appendix

Computation of the integral in the correction term in equation (19):

$$G_0 = \int_{-1}^{\xi_0} \frac{(1+x)(\alpha-x)}{(\beta-x)^{5/2}(x+\gamma)^{3/2}} dx, \qquad \beta > \xi_0, \quad \gamma > 1. \tag{33}$$

The key element of further calculations is the integral

$$\int \frac{dx}{(\gamma-x)^{1/2}(\beta+x)^{3/2}} = -\frac{2}{\beta+\gamma}\left(\frac{\gamma-x}{\beta+x}\right)^{1/2}, \tag{34}$$

which can be readily computed by change of variable $t = \dfrac{\gamma-x}{\beta+x}$ for $x \in (-\beta, \gamma)$.

We formally differentiate the integral (34) with respect to the parameter β to obtain

$$\int \frac{dx}{(\gamma-x)^{1/2}(\beta+x)^{5/2}} = -\frac{2}{3}\frac{(\gamma-x)^{1/2}(2x+3\beta+\gamma)}{(\beta+\gamma)^2(\beta+x)^{3/2}}. \tag{35}$$

Differentiating this further with respect to γ, we arrive at

$$\int \frac{dx}{(\gamma-x)^{3/2}(\beta+x)^{5/2}} = \frac{2}{3}\frac{(4x-3\gamma+\beta)(2x+3\beta+\gamma)+2(\gamma-x)(\beta+\gamma)}{(\beta+\gamma)^3(\gamma-x)^{1/2}(\beta+x)^{3/2}}. \tag{36}$$

Now notice that we can decompose (33) as

$$\begin{aligned} G_0 \quad = \quad & \int_{-\xi_0}^{1} \frac{dx}{(\beta+x)^{3/2}(\gamma-x)^{1/2}} + (\alpha-\beta+\gamma-1)\int_{-\xi_0}^{1} \frac{dx}{(\beta+x)^{5/2}(\gamma-x)^{1/2}} \\ & + (1-\gamma)(\gamma+\alpha)\int_{-\xi_0}^{1} \frac{dx}{(\beta+x)^{5/2}(\gamma-x)^{3/2}}, \end{aligned}$$

and so the integrals (34)-(36) team up to produce the result (20).

Computation of the integral in the correction term in equations (25), (27):

$$\widetilde{G}_1 := \int_C^{\infty} \frac{J_1(x)}{x^3} dx, \qquad C > 0. \tag{37}$$

In order to evaluate this integral, we will repeatedly employ a few well-known properties of Bessel functions [5], mainly recurrence formulas

$$\frac{1}{x}J_n(x) = \frac{1}{2n}\left(J_{n-1}(x) + J_{n+1}(x)\right), \tag{38}$$

$$J_n'(x) = \frac{1}{2}\left(J_{n-1}(x) - J_{n+1}(x)\right), \tag{39}$$

implying, in particular,

$$J_0'(x) = -J_1(x), \tag{40}$$

$$J_3(x) = \left(\frac{8}{x^2} - 1\right) J_1(x) - \frac{4}{x} J_0(x), \tag{41}$$

and also Bessel differential equation

$$x^2 J_n''(x) + x J_n'(x) + \left(x^2 - n^2\right) J_n(x) = 0 \quad \Leftrightarrow \quad \frac{1}{x} J_n'(x) = \left(\frac{n^2}{x^2} - 1\right) J_n(x) - J_n''(x). \tag{42}$$

We start by using (38) with $n = 1$ to compute the indefinite integral

$$\int \frac{J_1(x)}{x^3} dx = \frac{1}{2} \int \frac{J_0(x)}{x^2} dx + \frac{1}{2} \int \frac{J_2(x)}{x^2} dx. \tag{43}$$

The first term on the right we integrate by parts and use the differential equation (39) for $J_0(x)$ to obtain

$$\int \frac{J_0(x)}{x^2} dx = -\frac{J_0(x)}{x} + \int \frac{J_0'(x)}{x} dx = -\frac{J_0(x)}{x} - J_0'(x) - \int J_0(x)\, dx. \tag{44}$$

Application of the same strategy to the second term in the right-hand side of (43) is not immediately beneficial due to the presence of an extra term in the equation (39) for $n = 2$, however, it still yields

$$\int \frac{J_2(x)}{x^2} dx = -\frac{J_2(x)}{x} - J_2'(x) - \int J_2(x)\, dx + 4 \int \frac{J_2(x)}{x^2} dx$$

$$\Rightarrow \quad \int \frac{J_2(x)}{x^2} dx = \frac{1}{3} \left(\frac{J_2(x)}{x} + J_2'(x) + \int J_2(x)\, dx\right). \tag{45}$$

Now it is time to notice that $\int J_2(x)\, dx$ expresses in terms of $\int J_0(x)\, dx$, another ingredient we have. Indeed, from the integral representation of Bessel functions

$$J_n(x) = \frac{1}{\pi} \int_0^\pi \cos(nt - x \sin t)\, dt, \tag{46}$$

we directly get

$$\int J_n(x)\, dx = \frac{1}{\pi} \int_0^\pi \frac{\sin(x \sin t - nt)}{\sin t} dt = \frac{1}{\pi} \int_0^\pi \frac{\cos(nt) \sin(x \sin t)}{\sin t} dt - \frac{1}{\pi} \int_0^\pi \frac{\sin(nt) \cos(x \sin t)}{\sin t} dt,$$

and, in particular,

$$\int J_2(x)\, dx = \frac{1}{\pi} \int_0^\pi \frac{\left(1 - 2\sin^2 t\right) \sin(x \sin t)}{\sin t} dt - \frac{2}{\pi} \int_0^\pi \frac{\cos t \cos(x \sin t)}{\sin t} dt = \int J_0(x)\, dx - 2 J_1(x). \tag{47}$$

Now getting back to (43), we plug (44)-(45) and use (38)-(39) with $n = 2$ and (40) to arrive at

$$\int \frac{J_1(x)}{x^3} dx = -\frac{1}{2} \frac{J_0(x)}{x} + \frac{5}{8} J_1(x) - \frac{1}{24} J_3(x) - \frac{1}{2} \int J_0(x)\, dx + \frac{1}{6} \int J_2(x)\, dx.$$

From here, making use of (41) and (47), we obtain

$$\int \frac{J_1(x)}{x^3}dx = -\frac{1}{3}\left(\frac{J_0(x)}{x} - \left(1-\frac{1}{x^2}\right)J_1(x) + \frac{1}{2}\int J_0(x)\,dx\right). \tag{48}$$

It remains to compute the last integral term on the right, however, this can be done only in terms of other special functions using [5, (10.22.2)] with $\nu = 0$

$$\int J_0(x)\,dx = \frac{\pi}{2}x\left(J_0(x)H_{-1}(x) - J_{-1}(x)H_0(x)\right), \tag{49}$$

where Struve functions can be defined as

$$H_n(x) = \frac{n!}{(2n)!}(2x)^n\frac{2}{\pi}\int_0^{\pi/2}\cos^{2n}t\sin(x\sin t)\,dt, \tag{50}$$

in particular,

$$H_0(x) = \frac{2}{\pi}\int_0^{\pi/2}\sin(x\sin t)\,dt, \tag{51}$$

$$H_{-1}(x) = \frac{2}{\pi} - H_1(x) = \frac{2}{\pi}\left(1 - x\int_0^{\pi/2}\cos^2 t\sin(x\sin t)\,dt\right). \tag{52}$$

To compute the definite integral (37), we have to know the limiting behavior at infinity. To deduce it, we need representation of Struve functions in terms of modified Struve and Neumann functions, $K_n(x)$ and $Y_n(x)$, respectively, and their asymptotics as $x \to \infty$ [5, (11.2.5), (11.6.1)]

$$H_n(x) = K_n(x) + Y_n(x),$$

$$K_n(x) \simeq \frac{2^{n+1}n!}{\sqrt{\pi}(2n)!}x^{n-1} + \mathcal{O}\left(x^{n-3}\right),$$

$$Y_n(x) \simeq \sqrt{\frac{2}{\pi x}}\sin\left(x - \frac{n\pi}{2} - \frac{\pi}{4}\right) + \mathcal{O}\left(\frac{1}{x}\right).$$

Recalling also asymptotics of Bessel functions of the first kind for large values of x

$$J_n(x) \simeq \sqrt{\frac{2}{\pi x}}\cos\left(x - \frac{n\pi}{2} - \frac{\pi}{4}\right) + \mathcal{O}\left(\frac{1}{x}\right),$$

we can now evaluate

$$\begin{aligned}\lim_{x\to+\infty}\int\frac{J_1(x)}{x^3}dx &= -\frac{\pi}{6}\lim_{x\to+\infty}x\left(J_0(x)H_{-1}(x)-J_{-1}(x)H_0(x)\right)\\ &= -\frac{\pi}{6}\lim_{x\to+\infty}x\left[\frac{2}{\pi x}\cos^2\left(x-\frac{\pi}{4}\right)+\frac{2}{\pi x}\sin^2\left(x-\frac{\pi}{4}\right)\right]\\ &= -\frac{1}{3}.\end{aligned}$$

Therefore, employing (49) and (52), from (48), we finally conclude

$$\widetilde{G}_1=-\frac{1}{3}\left[1-\left(1+\frac{1}{C^2}\right)CJ_0(C)+\left(1-\frac{1}{C^2}\right)J_1(C)+\frac{\pi C}{2}\left(J_0(C)H_1(C)-J_1(C)H_0(C)\right)\right].$$

Computation of the integral in the correction term in equations (30), (32):

$$\widetilde{G}_2:=\int_C^\infty\frac{J_0(x)}{x^2}dx,\qquad C>0. \tag{53}$$

In fact, this integral has already been computed as part of calculations for (37). Indeed, the indefinite integral (44) reads

$$\int\frac{J_0(x)}{x^2}dx=-\frac{J_0(x)}{x}+J_1(x)-\int J_0(x)\,dx=-\frac{J_0(x)}{x}+J_1(x)-xJ_0(x)-\frac{\pi}{2}x\left(J_1(x)H_0(x)-J_0(x)H_1(x)\right).$$

As before,

$$\lim_{x\to+\infty}\int\frac{J_0(x)}{x^2}dx=-\frac{\pi}{2}\lim_{x\to+\infty}x\left(J_0(x)H_{-1}(x)-J_{-1}(x)H_0(x)\right)=-1,$$

and thus

$$\widetilde{G}_2=-1+\frac{J_0(C)}{C}-J_1(C)+CJ_0(C)+\frac{\pi}{2}C\left(J_1(C)H_0(C)-J_0(C)H_1(C)\right).$$

References

[1] B. Atfeh, L. Baratchart, J. Leblond, J. Partington, "Bounded Extremal and Cauchy-Laplace Problems on the Sphere and Shell", J. Fourier Anal. Appl., 16, 177-203, 2010.

[2] S. Axler, P. Bourdon, W. Ramey, "Harmonic Function Theory", Springer, 2001.

[3] L. Baratchart, D. P. Hardin, E. A. Lima, E. B. Saff and B. P. Weiss, "Characterizing kernels of operators related to thin-plate magnetizations via generalizations of Hodge decompositions", Inverse Problems, 29 (1), 2013.

[4] E. A. Lima, B. P. Weiss, L. Baratchart, D. P. Hardin and E. B. Saff, "Fast inversion of magnetic field maps of unidirectional planar geological magnetization", J. Geophys. Res.: Solid Earth, 118 (6), 2723-2752, 2013.

[5] F. W. J. Olver, D. W. Lozier, R. F. Boisvert, C. W. Clark, "NIST Handbook of Mathematical Functions", Cambridge University Press, 2010.

[6] W. Rudin, "Real and Complex Analysis", McGraw-Hill, 1987.